Field evaporation of semiconductors assisted by nonequilibrium phonon excitations

E. P. Silaeva, J. Houard, A. Hideur, G. Martel, and A. Vella*

Groupe de Physique des Matériaux UMR CNRS 6634, CORIA UMR CNRS 6614, Normandie Université, Université-INSA de Rouen, Avenue de l'Université, Boîte Postale 12, 76801 Saint Etienne du Rouvray, France

(Received 17 June 2015; revised manuscript received 18 September 2015; published 19 November 2015)

Laser-assisted field evaporation of materials is often interpreted as an equilibrium phenomenon that can be described in terms of a thermally assisted process due to the increase of the lattice temperature defined for equilibrium phonon distribution. Our simulations, taking into account nonequilibrium phonon distribution, produced by femtosecond laser radiation, and coupled carrier-phonon kinetics in the sample, show that the evaporation process is assisted by hot phonons. An out-of-thermal-equilibrium phenomenon on the picosecond time scale is thus demonstrated in the case of femtosecond-laser-assisted field evaporation of semiconductors. It is experimentally confirmed by atom-probe measurements using an original double-pulse correlation setup.

DOI: 10.1103/PhysRevB.92.195307 PACS number(s): 79.70.+q, 79.20.La, 05.70.Ln, 82.53.Mj

I. INTRODUCTION

Huge electric field can be used to softly destroy materials, atom by atom, by field evaporation, i.e., ion desorption from the surface of the material induced by a dc field of several volts per angstrom. Moreover, the field-evaporation process can be triggered and controlled in time by ultrafast laser pulses. The laser-assisted field evaporation is the fundamental process of atom-probe tomography (APT). This technique is able to image materials with 3D subnanometric resolution. For this reason, APT is currently being applied more and more in different domains of nanoscale science and technology, such as metallurgy, electronics, geosciences, and catalysis [1–7]. Even though APT was proven to be very powerful for providing the detailed structure of materials with truly quantitative elemental measurement, these results are far from being straightforward. APT analysis of nanostructures can simply fail, or their composition measurements can strongly depend on the experimental conditions [8,9]. These difficulties arise from the complexity of the laser-assisted field-evaporation process. In the case of semiconductors and dielectrics, the exact time scale and the mechanisms of this process are still not known [10].

It was recently proved that, under high dc field, a laser pulse is efficiently absorbed at the surface of a semiconductor, on a thickness of a few nanometers, even at the sub-band-gap photon energies due to the strong band-gap shrinkage under high dc field [11]. Moreover, the recent double-pulse correlation APT experiment on silicon has shown that the field evaporation has a picosecond response time [12]. From all these observations, the question that arises is, Can the classical thermodynamics provide an accurate microscopic description of ultrafast processes at nanometric scale that are dynamically brought far from equilibrium?

This kind of question is also arising in the community of ultrafast and hot chemistry, particularly concerning the molecular absorption/desorption on surfaces of nanomaterials for sensing applications. For example, the absorption/desorption of gas molecules can influence the electrical and optical properties of graphene-based field-effect transistors [13]. However, in all the works concerning the photodesorption/evaporation of atoms from solid surfaces, only laser-induced electronic excitations are believed to play a major role [14]. In this work, we demonstrate direct evidence of the desorption induced by nonequilibrium phonon excitations, an unexplored mechanism in the domains mentioned above. This mechanism is a good candidate to explain some puzzling experimental results on photodesorption and to help to significantly improve the APT. In particular, we show that the classical thermodynamics can still describe well the ultrafast nonequilibrium photodesorption/evaporation if an effective temperature is introduced, corresponding to the nonequilibrium or hot-phonon distribution. This effective temperature is much higher than the lattice temperature, and it can be at the origin of surface diffusion, which can cause the recently reported deviations from stoichiometry in APT analysis [9,15,16]. The temporal evolution of the effective temperature is probed by time-resolved measurements using laser-assisted APT. A model taking into account the nonequilibrium phonon distribution, produced by the relaxation of hot laser-generated carriers, is developed. The model includes transport equations for carrier density and temperature and describes the generation and decay of nonequilibrium optical phonons. Then, the effective temperature is introduced as a measure of energy density in the nonequilibrium phonon bath. Good agreement is found between the prediction of our model and the experimental results, supporting the hot-phonon-assisted field-evaporation mechanism of semiconductors and dielectrics.

II. EXPERIMENTAL SETUP AND RESULTS

In laser-assisted APT, a semiconductor sample shaped as a nanotip is biased at high positive voltage of 5–10 kV. The high dc field generated at the tip apex ($E_{DC} \approx 20$–30 V/nm) leads to the ionization and desorption of atoms, i.e., field evaporation, from the surface of the semiconductor. The field-evaporation process is triggered using a femtosecond laser pulse [17]. Experiments are performed in ultrahigh vacuum ($<10^7$ Pa), and the sample is cooled down to cryogenic temperature ($T_0 = 80$ K). The laser system is an amplified Ti : sapphire laser (wavelength $\lambda = 800$ nm, frequency 1 kHz, pulse duration 40 fs, pulse energy up to 2.5 mJ/pulse). Using a nonlinear crystal, the wavelength is shifted down

*angela.vella@univ-rouen.fr

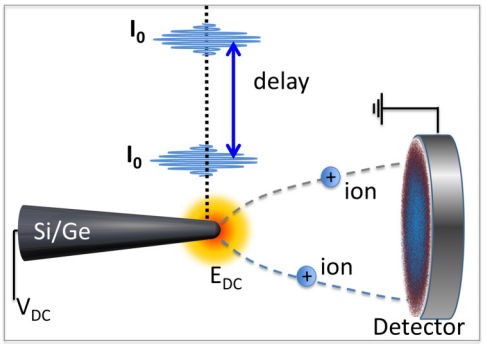

FIG. 1. (Color online) Schematic representation of the experimental time-resolved setup in the atom-probe chamber.

to $\lambda = 400$ nm by second-harmonic generation. Using an autocorrelation setup, two identical laser pulses with a variable temporal delay are focused on the tip apex with a spot diameter of 100 μm. Their linear polarization is set parallel to the symmetry axis of a cone-shaped tip to ensure maximum laser absorption efficiency at 400 nm [18]. The laser energy per pulse is varied between 100 and 700 nJ. The schematic representation of the experimental setup is shown in Fig. 1. More details on the setup can be found in Ref. [19].

The evaporation rate (i.e., number of atoms removed from the surface and detected as ions per laser pulse) is measured by varying the delay from 0.15 to 19 ps at an equivalent displacement speed of 0.025 mm/s. It is worth noting that the smallest delay was set to 150 fs to avoid any optical interaction of the two laser pulses. Figure 2 shows the evolution of the total number of detected ions per each *double-pulse sequence* N_{ion} from Ge and Si as a function of the delay between the pulses. For each value of the laser peak intensity, the voltage applied to the sample was adjusted in order to obtain N_{ion} of 0.07 (0.03) atom/pulse at the fixed delay of 19 ps (7 ps) for Ge (Si). To evaluate the tip blunting due to the evaporation

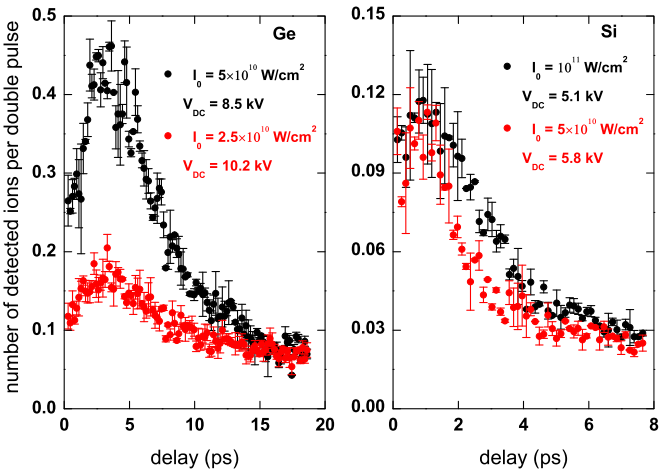

FIG. 2. (Color online) Number of detected ions per double pulse N_{ion} as a function of the delay between two 40-fs laser pulses at 400-nm wavelength for Ge and Si samples at different values of peak laser intensity I_0 and bias V_{DC}. I_0 and V_{DC} are chosen to keep the same evaporation rate at the longest delay.

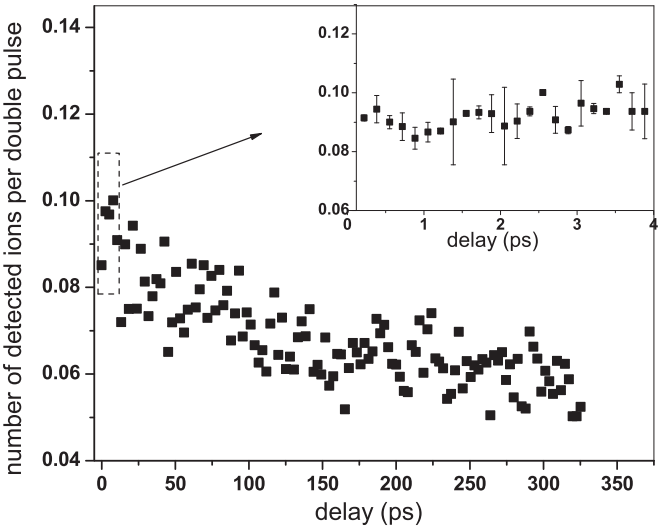

FIG. 3. Number of detected ions per double pulse N_{ion} as a function of the delay between two 40-fs laser pulses at 400-nm wavelength for an Al sample with peak laser intensity of each pulse $I_0 = 2.5 \times 10^{11}$ W/cm^2 and bias $V_{DC} = 6.2$ kV. The inset shows a zoom on N_{ion} at short time delays.

process, the measurements are performed successively in the two directions of the stage of the autocorrelation setup. No significant difference between directions and thus no tip blunting are observed. The average of two directions is shown in Fig. 2.

For long delays between pulses, N_{ion} decays monotonically as a function of the delay, with a short decay time of about 7 ps for Ge and 3 ps for Si, as already reported in Ref. [12]. However, for shorter delays, N_{ion} increases as a function of the delay, revealing a maximum of the evaporation rate around 3 ps for Ge and 1 ps for Si. Such nonmonotonic behavior has never been reported before for metallic samples [20]. To prove that for semiconductors it is related to the coupling of carriers to optical phonons and their nonequilibrium behavior, we performed an experiment on an Al tip using the same experimental conditions in terms of laser parameters (wavelength, polarization, pulse duration) and detection rate. The results are reported in Fig. 3. As expected for metallic samples [20,21], the decay time of the number of detected ions N_{ion} is about 150 ps, much longer than in the case of Si and Ge. Moreover, the behavior of N_{ion} for Al is monotonic and does not show any maxima at short delays.

III. THEORETICAL MODEL

The nonmonotonic behavior of ion yield as a function of delay between femtosecond laser pulses, as reported in Fig. 2, is often observed in pump-probe or double-pulse correlation experiments on laser ablation and photodesorption of semiconductors [22–24]. It is usually due to the fact that the first laser pulse excites the sample and changes its optical properties. The second laser pulse is thus absorbed differently compared to the first one. Such first-pulse-induced excitation evolves in time due to electronic and thermal relaxation. Thus, the absorption of the second pulse depends strongly on the

delay between pulses. The optical properties of the laser-excited semiconductor change due to state and band filling, renormalization of the band structure, and the laser-generated free-carrier response [22,23]. It can also be related to the coupling of the second pulse with the ultrafast melting process induced by the first pulse [24]. Lattice heating caused by the first pulse can also increase the absorption coefficient of the semiconductor [25].

In our previous calculations [12], all these processes were taken into account. However, in laser-assisted field evaporation laser intensity is relatively low, and less than 10^{20} cm^{-3} carriers are generated, which is not sufficient to cause any band filling or band structure renormalization or to induce strong thermal effects causing any phase transformations of the semiconductor. For these processes to be significant, one needs densities of about 10^{22} cm^{-3} carriers. Additionally, our experiments are performed with photon energy well above the semiconductor band gap when its absorption is already very strong, and the first laser pulse can change it only negligibly. As a result, our previous theoretical work showed only the fast monotonic decay of $N_{\rm ion}$ that was associated with a fast heating and cooling of the lattice due to the confinement of the absorption at the tip apex under the strong dc field [12]. The model of the lattice heating and cooling was developed considering an equilibrium phonon distribution. This model cannot reproduce the increase of $N_{\rm ion}$ for a short delay of a few picoseconds, as reported experimentally. Only a fundamentally different evaporation mechanism can explain such nonmonotonic experimental behavior. Here we propose another mechanism of nonequilibrium ultrafast evaporation and improve our previous model by taking into account the nonequilibrium phonon distribution.

First, the laser-tip interaction is modeled by numerically solving Maxwell equations using a commercial-grade simulator based on the finite-difference time-domain method [26] in the three-dimensional (3D) geometry of the tip. The shape of a real tip is approximated by a semisphere of radius 50 nm on a cone of angle 5°. The calculated absorbed power density along the tip axis of symmetry, averaged over the tip cross section, is reported in Fig. 4 for Ge and Si at 400-nm wavelength (black lines). The transient response of the semiconductor tip to the laser illumination is then studied using a one-dimensional (1D) model along the axial direction of the tip. Below we give a qualitative explanation of experimental observations, for which such a simplified 1D model is sufficient.

Concerning the dc field contribution, it was recently proved that the dc field is screened at the surface of semiconductor and dielectric nanotips [11] and thus has a negligible effect on the laser-excited carrier motion inside the tip, as was proposed previously [27,28]. Moreover, the dc field, screened within a few nanometers at the tip apex, can strongly increase its absorption [11]. The change of absorption due to the dc field is related to the decrease of the band gap in high dc field, as calculated for Si in Ref. [29]. At the field of 25 V/nm the expected band-gap shrinkage of Si is about $\Delta\mathcal{E}_{\rm gap} = 0.6$ eV. The change of the absorption coefficient for a photon of energy $\hbar\omega$ due to the band-gap shrinkage can be estimated from the corresponding shift of the absorption spectrum of Si: $\alpha(\hbar\omega + \Delta\mathcal{E}_{\rm gap})$ with $\hbar\omega = 3.1$ eV for the given wavelength $\lambda = 400$ nm [11,30]. In Fig. 4 this field-assisted contribution to

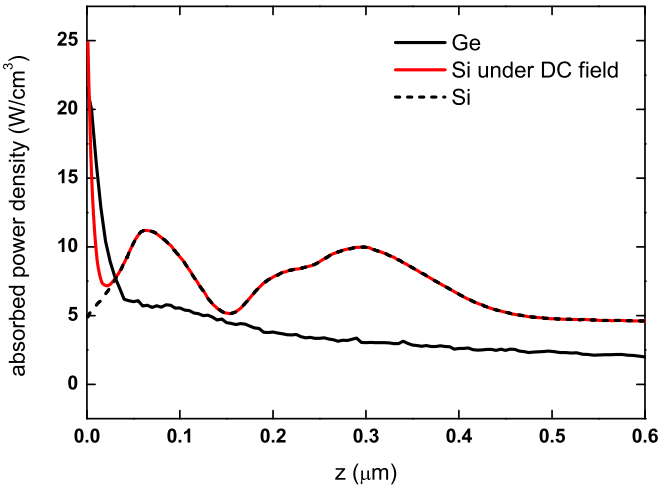

FIG. 4. (Color online) Absorbed power density along the tip axis of symmetry z for the laser radiation with incident intensity of 1 W/m^2 and wavelength 400 nm inside Ge (solid black line), inside Si (dashed black line), and inside Si taking into account absorption enhancement due to high dc field (solid red line).

the absorption of Si is shown in red. At the very surface at $z = 0$ the absorption coefficient with dc field is 5 times higher than that without the field. A similar band-gap shrinkage is expected for Ge subjected to a high dc field. However, the corresponding shift of the absorption spectrum ($\Delta\mathcal{E}_{\rm gap} > 0.4$ eV) results in a negligible change of the absorption coefficient for a photon energy of 3.1 eV. Thus, we neglect the effect of the field on the absorption profile of the Ge tip.

The model of generation of carriers and phonons inside a semiconductor illuminated by a laser pulse is based on the approach developed by Othonos *et al.* [31]. For Ge (without external dc field) the evolution in space and time of the laser-generated electron density n_e and hole density n_h is modeled by the continuity equations:

$$\frac{\partial n_{e,h}}{\partial t} + \frac{1}{e}\frac{\partial}{\partial z}J_{e,h} = S_{e,h} - R_A, \tag{1}$$

where e is the absolute value of electronic charge. The electron and hole current densities J_e and J_h, respectively, are given by

$$J_{e,h} = eD_{e,h}\frac{\partial n_{e,h}}{\partial z}, \tag{2}$$

where the diffusion coefficients for electrons D_e and for holes D_h are considered for Fermi-Dirac statistics of carriers [27]. The carrier loss is caused by Auger recombination at the rate $R_A = C_A n_e^3$, with $C_A = 1.1 \times 10^{-31}$ cm^{-6} s^{-1} for Ge [32]. The spatial and temporal evolution of the source of carriers $S_{e,h}$ is given by

$$S_{e,h}(z,t) = \frac{P_{\rm abs}(z)I_0}{\hbar\omega}\left[e^{-\frac{t^2}{\tau_p^2}4\ln 2} + e^{-\frac{(t-\delta t)^2}{\tau_p^2}4\ln 2}\right], \tag{3}$$

where $P_{\rm abs}(z)$ is the density of absorbed power shown in Fig. 4 and I_0 is the laser-pulse peak intensity. The exponential factors describe the temporal profile of a laser-pulse sequence consisting of two pulses with full width at half maximum duration τ_p and time separation δt. The kinetics of electron, hole, and lattice temperatures T_e, T_h, and T_L, respectively, is

described by the following continuity equations:

$$\frac{\partial}{\partial t}(C_e T_e) = \frac{\partial}{\partial z} k_e \frac{\partial T_e}{\partial z} + S_e \frac{m_h^*}{m_h^* + m_e^*}(\hbar\omega - \mathcal{E}_{\text{gap}}) + \frac{\mathcal{E}_{\text{gap}}}{2} R_A - L_e,$$

$$\frac{\partial}{\partial t}(C_h T_h) = \frac{\partial}{\partial z} k_h \frac{\partial T_h}{\partial z} + S_h \frac{m_e^*}{m_h^* + m_e^*}(\hbar\omega - \mathcal{E}_{\text{gap}}) + \frac{\mathcal{E}_{\text{gap}}}{2} R_A - L_h,$$

$$\frac{\partial}{\partial t}(C_L T_L) = \frac{\partial}{\partial x} k_L \frac{\partial T_L}{\partial x} + L_e + L_h. \quad (4)$$

These equations take into account the thermal conduction and the contribution to carrier energy related to the Auger recombination process. The initial excess energy of carriers $(\hbar\omega - \mathcal{E}_{\text{gap}})$ is divided between electrons and holes according to their effective masses m_e^* and m_h^*. The carrier thermal conductivities k_e and k_h and heat capacities C_e and C_h depend on carrier density and Fermi-Dirac statistics [27]. The lattice thermal conductivity k_L is temperature dependent and takes into account the nanowirelike shape of the tip [33]. The terms L_e and L_h describe the energy transfer between electrons and phonons and holes and phonons, respectively.

The energy of hot electrons and holes is relaxed by emitting nonequilibrium optical and acoustic phonons. The temporal evolution of phonon occupation number n_q is obtained by solving the following equation:

$$\frac{\partial n_q}{\partial t} = \left(\frac{\partial n_q}{\partial t}\right)_{\text{tot}}^{\text{gen}} - \left(\frac{n_q - n_q^{eq}}{\tau_{ph}}\right), \quad (5)$$

where n_q^{eq} is the equilibrium phonon occupation number, tot indicates the total contribution from relaxing electrons and holes, and $\tau_{ph} = 8$ ps is the nonequilibrium phonon decay time measured experimentally [34]. Energy loss by hot carriers to acoustic phonons is generally small compared with the loss due to optical phonons [35]. Thus, it is neglected in this study. The generated optical phonons eventually decay into acoustic phonons [36,37]. The energy-loss rate of hot carriers due to optical-phonon processes is obtained by integrating the corresponding optical-phonon generation rate $(\partial n_q/\partial t)^{\text{gen}}$ over all wave vectors. The generation rate of the transverse or longitudinal optical phonons with wave vector q is given by [31,34]

$$\left(\frac{\partial n_q}{\partial t}\right)_{e,h}^{\text{gen}} = n_{e,h}\left(\frac{\pi}{2}\right)^{1/2} \frac{\mathcal{D}_{e,h}^2}{\rho \mathcal{E}_{ph} q}\left(\frac{m^*}{k_B T_{e,h}}\right) \times \frac{e^{x_0 - x/2} - e^{x/2}}{e^{x_0} - 1} e^{x_1}, \quad (6)$$

where $x_0 = \mathcal{E}_{ph}/k_B T_L, x = \mathcal{E}_{ph}/k_B T_{e,h}, x_1 = -\hbar^2 x(m^{*2}\mathcal{E}_{ph}/\hbar^4 q^2 + q^2/4\mathcal{E}_{ph})/2m^*$, $\mathcal{D}_{e,h}$ is the optical deformation-potential constant, $\mathcal{E}_{ph}$ is the optical-phonon energy, and ρ is the density of the semiconductor. Multiplying this equation by $\mathcal{E}_{ph}$ and integrating it over all wave vectors gives, for the energy relaxation rate due to a particular phonon branch,

$$\left\langle \frac{dE}{dt} \right\rangle_{op} = -n_{e,h}\left(\frac{2}{\pi}\right)^{1/2} \frac{\mathcal{D}_{e,h}^2 m^{*3/2}}{\pi \hbar^2 \rho}(k_B T_{e,h})^{1/2} \times \frac{e^{x_0 - x} - 1}{e^{x_0} - 1} \frac{x}{2} e^{x/2} K_1(x/2), \quad (7)$$

where K_1 is the modified Bessel function of the second kind. We consider both intravalley and intervalley scattering processes. The deformation-potential constants and effective masses associated with different valleys are taken from Refs. [31,38]. The terms L_e and L_h are found by summing the energy relaxation rates over the various phonon modes.

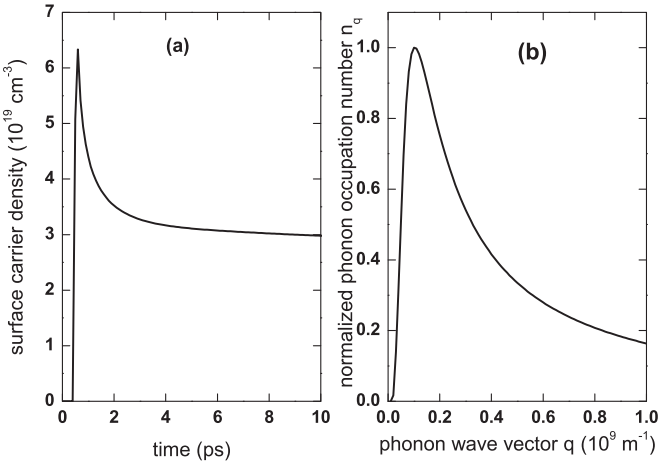

FIG. 5. (a) Surface-carrier-density temporal evolution after the arrival of a 40-fs single laser pulse with maximum intensity $I_0 = 2.5 \times 10^{10}$ W/cm^2 at 0.5 ps; (b) nonequilibrium optical-phonon population as a function of phonon wave vector generated by this pulse in Ge.

Right after the laser pulse of intensity $I_0 = 2.5 \times 10^{10}$ W/cm^2, the carrier density at the surface of the tip is about 7×10^{19} cm^{-3} [Fig. 5(a)], and carrier temperature is about 12 000 K for electrons and 5500 K for holes. These hot carriers relax their energy by emitting the optical phonons in the whole range of wave vectors [Fig. 5(b)]. We assume that the phonons with the highest occupation number will influence the field evaporation the most and thus consider the phonons with wave vector $q = 10^8$ m^{-1}, corresponding to the maximum in Fig. 5. The temporal evolution of the occupation number of phonons with $q = 10^8$ m^{-1} is shown in Fig. 6(a). The energy of the optical phonons in Ge is 37.2 meV [34].

In the case of the silicon sample, the calculations have been performed taking into account the dc field. In such a model, the carrier evolution is described by Eq. (1) with hole and electron currents given by

$$J_h = e\mu_h E n_h + eD_h \frac{\partial n_h}{\partial z}, \quad J_e = e\mu_e E n_e - eD_e \frac{\partial n_e}{\partial z}, \quad (8)$$

with the field $E = -\partial V/\partial z$. The potential V is found by solving the Poisson equation:

$$\frac{\partial}{\partial z}\varepsilon_r\left(\frac{\partial V}{\partial z}\right) = -\frac{e}{\varepsilon_0}(n_h - n_e), \quad (9)$$

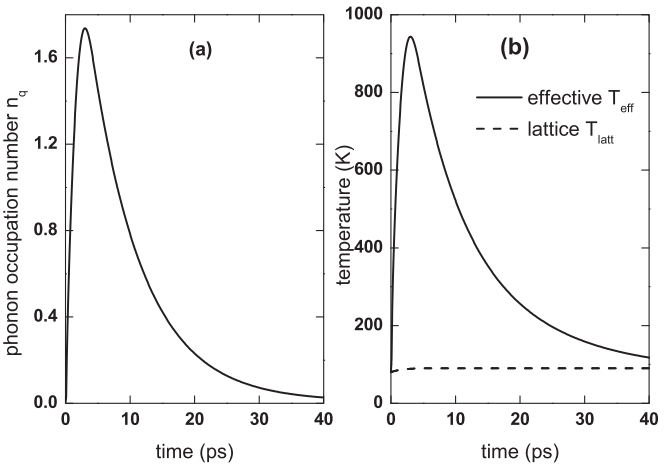

FIG. 6. Temporal evolution of (a) the nonequilibrium optical-phonon occupation number and (b) the effective phonon temperature (solid line) and lattice temperature (dashed line) at the surface of the Ge tip after the illumination by a single 40-fs laser pulse with $I_0 = 2.5\,\mathrm{W/cm^2}$ at 400-nm wavelength. The maximum of pulse intensity is at 0.5 ps.

where $\varepsilon_r = 11.7$ is the dielectric constant of Si and ε_0 is the vacuum permittivity. To reproduce the same spatial profiles of the field and potential in one dimension as in a real 3D tip along its axis of symmetry, the 1D geometry of the system is represented by a short vacuum region (200 nm) and a long Si "line" (10 μm length); a positive potential difference $V_{DC} = 5.1$ kV is applied between the ends. Such a 1D model is valid for 3D spherical geometries with a radius of curvature not much less than 20 nm [39]. In the experiment the dc voltage is applied much earlier than the laser illumination. Thus, in the calculation for Si the laser pulse arrives at the tip with a delay of a few microseconds. Before the arrival of the laser pulse the free electrons and holes inside the tip move according to Eqs. (1), (8), and (9) with $S_{e,h} = 0$ and initial carrier density $n_{e,h} = 10^{14}\ \mathrm{cm^{-3}}$ (Ref. [40]). The chosen delay is enough for the initial carriers to reach steady-state distribution, leading to the screening of the field inside the tip and the accumulation of high hole density at the tip apex [28]. For given parameters, the field at the Si surface reaches $E_{DC} = 25$ V/nm after the screening.

All material parameters including the mobilities $\mu_{e,h}$ are taken from Refs. [38,41]. The energy of optical phonons is 62 meV in Si [41,42], and the lifetime of nonequilibrium optical phonons is reported to be about 1 ps for given laser-generated carrier densities [43]. The phonon wave vector is taken to be $q = 10^8\ \mathrm{m^{-1}}$.

To understand the role of this rapidly evolving high density of nonequilibrium phonons on the field-evaporation process, we introduce an "effective phonon temperature" T_{eff} as a measure of energy density in a nonequilibrium-phonon bath, defined by [44]

$$n_q = \frac{1}{\exp\left(\frac{\mathcal{E}_{ph}}{k_B T_{\mathrm{eff}}}\right) - 1}, \tag{10}$$

with $\mathcal{E}_{ph} = 37.2$ meV for Ge and $\mathcal{E}_{ph} = 62$ meV for Si. The temporal evolution of the effective phonon temperature corresponding to $n_q(t)$ in Fig. 6(a) is reported in Fig. 6(b). The effective temperature is thus much higher and decreases much faster than the lattice temperature reported in Fig. 6(b). Then the number of detected ions can be obtained using an Arrhenius-type equation [17]:

$$N_{\mathrm{ion}} = \kappa \exp\left(-Q/k_B T_{\mathrm{eff}}\right), \tag{11}$$

where κ depends on the number of kink-site atoms at the tip surface, surface atom vibration frequency, dc field, duration of the evaporation during each pulse, and detector efficiency. The activation energy Q is on the order of several electron volts. It depends on dc field. During laser-induced excitations, the dc field at the surface can fluctuate due to the fluctuations in the ion flux and free-carrier dynamics. However, it was shown that dc field fluctuations are less than 0.1% [40]. Thus, for each set of parameters (laser intensity and dc voltage) the activation energy is taken as independent of time delay. Note also that the Arrhenius equation is commonly used to describe the dependence of ion yield on lattice temperature, especially for metals. Here we propose to replace the lattice temperature by the effective phonon temperature to be able to account for fast nonequilibrium processes in which the lattice temperature is not well defined.

IV. DISCUSSION

To reproduce the experimental result we simulated the response of effective temperature to two laser pulses separated by a delay δt. The simulation has been repeated several times by varying the delay from 0.3 to 19 ps with a step of 0.15 ps. Then, ideally, one should integrate the simulated evaporation rate over time (from 0 to ∞) for each time delay to compare with the experiment in which the total number of detected ions per double pulse was measured. However, since the behavior of the evaporation process is

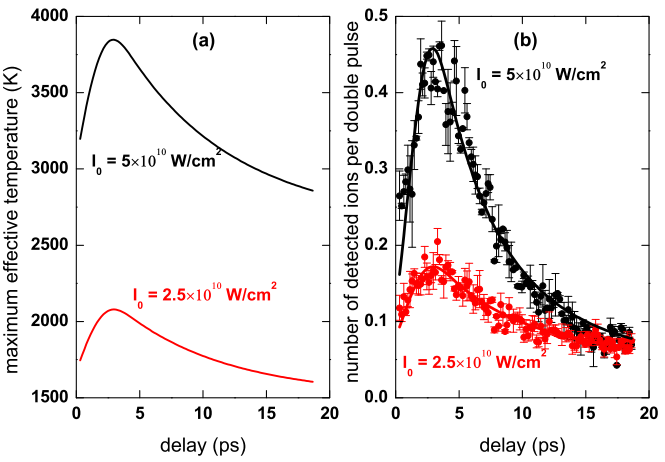

FIG. 7. (Color online) (a) Maximum effective phonon temperature reached at the surface of the Ge tip after being illuminated by two laser pulses separated by a delay δt with peak intensity I_0, calculated theoretically. (b) Number of detected ions per double pulse calculated using Eq. (11) with maximum effective temperature from (a) with a set of fitting parameters $\kappa = 77 \pm 11$ and $Q = 1.70 \pm 0.04$ eV (black solid line) and $\kappa = 4.3 \pm 0.5$ and $Q = 0.58 \pm 0.02$ eV (red solid line). Experimental points are shown by dots.

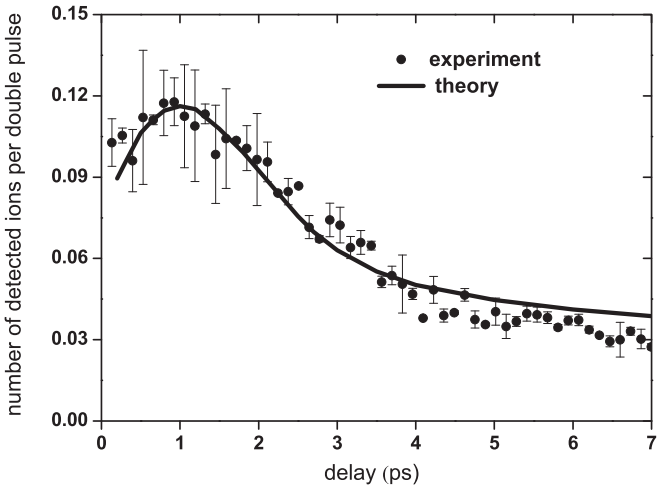

FIG. 8. Number of detected Si ions calculated using Eq. (11) with maximum effective temperature found from the solution of Eqs. (1)–(7) for different delays between two pulses (solid black line). The fitting parameters are $\kappa = 42 \pm 23$ and $Q = 1.47 \pm 0.14$ eV. Experimental points are shown by dots. Laser pulse intensity is $I_0 = 10^{11}$ W/cm^2; voltage is $V_{DC} = 5.1$ V.

exponential, most of the ions are emitted at the maximum effective temperature $T_{\rm eff}^{\rm MAX}$; hence, only the variation of the maximum temperature of the tip as a function of the delay can be considered, thus making the calculations simpler. The dependence of $T_{\rm eff}^{\rm MAX}$ on the delay for different laser intensities is shown in Fig. 7(a) and demonstrates features related to a strongly nonlinear dependence of the phonon occupation number on carrier density and temperature. The best fit of the experimental $N_{\rm ion}(\delta t)$ versus theoretical $T_{\rm eff}^{\rm MAX}(\delta t)$ with an Arrhenius function [see Eq. (11)] gives $\kappa = 77 \pm 11$ and $Q = 1.70 \pm 0.04$ eV for $I_0 = 5 \times 10^{10}$ W/cm^2 and $\kappa = 4.3 \pm 0.5$ and $Q = 0.58 \pm 0.02$ eV for $I_0 = 2.5 \times 10^{10}$ W/cm^2, thus showing a rather good qualitative agreement between experiment and theory [Fig. 7(b)]. The field-dependent values of Q and κ are different for different laser intensities because the dc field values were also changed to keep $N_{\rm ion}$ the same at long delays (see Fig. 2) [45].

The calculated number of detected ions per double pulse in the case of the Si sample for $I_0 = 10^{11}$ W/cm^2 is shown in Fig. 8. The best fit with the Arrhenius function gives $\kappa = 42 \pm 23$ and $Q = 1.47 \pm 0.14$ eV, thus demonstrating a reasonable agreement between theory and experiment. In contrast to Ge the decrease of laser intensity does not change significantly the behavior of $N_{\rm ion}$ as a function of delay for Si (see Fig. 2), both experimentally and theoretically. It is related to the difference in the residual dc field and carrier dynamics influenced by this field inside Ge and Si samples. Although the dc field is strongly screened inside the semiconductors, there is always a high dc field at the surface (inside a few-nanometer layer) and a low residual dc field inside the sample volume related to a voltage drop between the sample base and apex. This voltage drop comes from nonzero resistivity of the materials and is about a few volts for Si [40]. The related residual field of a few volts/micron influences carrier dynamics. The Ge sample has lower band gap and lower resistivity and thus lower residual field, which influences carrier dynamics negligibly. Additionally, the position of the maximum is different for Ge and Si because the optical phonons have different lifetimes: 8 ps in Ge and 1 ps in Si.

Note that we used a 1D theoretical model that disregards the transverse carrier and heat transport. Even with such a simplification, fairly good agreement with experiments is demonstrated. This is an indication that the transverse processes are most likely not significant in hot-phonon-induced field evaporation due to its much longer time scale. A full three-dimensional model is, however, required to verify this statement and is the subject of our future work.

V. SUMMARY

In summary, we studied the response of a semiconductor atom-probe tip to a femtosecond laser pulse using time-resolved measurements. We showed that nonequilibrium phonon processes have to be taken into account to explain the evolution of the field-evaporation rate at a picosecond time scale. Good qualitative agreement is found between the experimental and theoretical results using an accurate kinetic model, taking into account the field evaporation triggered by hot optical phonons that are emitted by hot laser-generated carriers and whose lifetime is on the order of several picoseconds. A hot-phonon-assisted mechanism is thus suggested to explain the laser-assisted field evaporation of semiconductors and dielectrics. This mechanism has to be kept in mind in the interpretation of data from atom-probe tomography, as well as from other photo-desorption techniques involving femtosecond laser pulses.

ACKNOWLEDGMENTS

This work was supported by the French l'Agence Nationale de la Recherche (ANR), through the program Investissements d'Avenir (ANR-10-LABX-09-01), LabEx EMC3, the ASAP project, and CAMECA Instruments, Inc. (RING-APT project).

[1] T. F. Kelly and D. J. Larson, Annu. Rev. Mater. Res. **42**, 1 (2012).
[2] P. V. Liddicoat, X.-Z. Liao, Y. Zhao, Y. Zhu, M. Y. Murashkin, E. J. Lavernia, R. Z. Valiev, and S. P. Ringer, Nat. Commun. **1**, 63 (2010).
[3] K. Biswas, J. He, I. D. Blum, C.-I. Wu, T. P. Hogan, D. N. Seidman, V. P. Dravid, and M. G. Kanatzidis, Nature (London) **489**, 414 (2012).
[4] L. M. Gordon and D. Joester, Nature (London) **469**, 194 (2011).
[5] L. Rigutti, I. Blum, D. Shinde, D. Hernandez-Maldonado, W. Lefebvre, J. Houard, F. Vurpillot, A. Vella, M. Tchernycheva, C. Durand, J. Eymery, and B. Deconihout, Nano Lett. **14**, 107 (2014).
[6] O. Moutanabbir, D. Isheim, H. Blumtritt, S. Senz, E. Pippel, and D. N. Seidman, Nature (London) **496**, 78 (2013).

[7] J. W. Valley, A. J. Cavosie, T. Ushikubo, D. A. Reinhard, D. F. Lawrence, D. J. Larson, P. H. Clifton, T. F. Kelly, S. A. Wilde, D. E. Moser, and M. J. Spicuzza, Nat. Geosci. **7**, 219 (2014).
[8] A. Devaraj, R. Colby, F. Vurpillot, and S. Thevuthasan, J. Phys. Chem. Lett. **5**, 1361 (2014).
[9] L. Mancini, N. Amirifar, D. Shinde, I. Blum, M. Gilbert, A. Vella, F. Vurpillot, W. Lefebvre, R. Lard, E. Talbot, P. Pareige, X. Portier, A. Ziani, C. Davesnne, C. Durand, J. Eymery, R. Butt, J.-F. Carlin, N. Grandjean, and L. Rigutti, J. Phys. Chem. C **118**, 24136 (2014).
[10] D. K. Schreiber, A. N. Chiaramonti, L. M. Gordon, and K. Kruska, Appl. Phys. Lett. **105**, 244106 (2014).
[11] E. P. Silaeva, L. Arnoldi, M. L. Karahka, B. Deconihout, A. Menand, H. J. Kreuzer, and A. Vella, Nano Lett. **14**, 6066 (2014).
[12] A. Vella, E. P. Silaeva, J. Houard, T. E. Itina, and B. Deconihout, Ann. Phys. (Berlin, Ger.) **525**, L1 (2013).
[13] S. M. Hornett, M. Heath, D. W. Horsell, and E. Hendry, Phys. Rev. B **90**, 081401 (2014).
[14] H. Tamura, M. Tsukada, K. P. McKenna, A. L. Shluger, T. Ohkubo, and K. Hono, Phys. Rev. B **86**, 195430 (2012).
[15] A. Devaraj, R. Colby, W. P. Hess, D. E. Perea, and S. Thevuthasan, J. Phys. Chem. Lett. **4**, 993 (2013).
[16] T. Kinno, M. Tomita, T. Ohkubo, S. Takeno, and K. Hono, Appl. Surf. Sci. **290**, 194 (2014).
[17] M. K. Miller and R. Forbes, *Atom Probe Tomography: The Local Electrode Atom Probe* (Springer, New York, 2014).
[18] A. Vella, N. Sevelin-Radiguet, J. Houard, and B. Deconihout, Appl. Surf. Sci. **258**, 9202 (2012).
[19] A. Vella, M. Gilbert, A. Hideur, F. Vurpillot, and B. Deconihout, Appl. Phys. Lett. **89**, 251903 (2006).
[20] A. Vella, J. Houard, F. Vurpillot, and B. Deconihout, Appl. Surf. Sci. **255**, 5154 (2009).
[21] F. Vurpillot, J. Houard, A. Vella, and B. Deconihout, J. Phys. D **42**, 125502 (2009).
[22] K. Sokolowski-Tinten and D. von der Linde, Phys. Rev. B **61**, 2643 (2000).
[23] A. J. Sabbah and D. M. Riffe, Phys. Rev. B **66**, 165217 (2002).
[24] H. Dachraoui and W. Husinsky, Phys. Rev. Lett. **97**, 107601 (2006).
[25] D. L. Kwong and D. M. Kim, J. Appl. Phys. **54**, 366 (1983).
[26] Lumerical, FDTD SOLUTIONS, http://www.lumerical.com/tcad-products/fdtd/.
[27] E. P. Silaeva, A. Vella, N. Sevelin-Radiguet, G. Martel, B. Deconihout, and T. E. Itina, New J. Phys. **14**, 113026 (2012).
[28] E. P. Silaeva, N. S. Shcheblanov, T. E. Itina, A. Vella, J. Houard, N. Sevelin-Radiguet, F. Vurpillot, and B. Deconihout, Appl. Phys. A **110**, 703 (2013).
[29] E. P. Silaeva, M. Karahka, and H. Kreuzer, Curr. Opin. Solid State Mater. Sci. **17**, 211 (2013).
[30] E. D. Palik, *Handbook of Optical Constants of Solids* (Academic Press, San Diego, 1998).
[31] A. Othonos, H. M. van Driel, J. F. Young, and P. J. Kelly, Phys. Rev. B **43**, 6682 (1991).
[32] D. H. Auston, C. V. Shank, and P. LeFur, Phys. Rev. Lett. **35**, 1022 (1975).
[33] N. Mingo, L. Yang, D. Li, and A. Majumdar, Nano Lett. **3**, 1713 (2003).
[34] J. Young, K. Wan, and H. van Driel, Solid State Electron. **31**, 455 (1988).
[35] M. Artaki and P. J. Price, J. Appl. Phys. **65**, 1317 (1989).
[36] A. Othonos, J. Appl. Phys. **83**, 1789 (1998).
[37] M. Kazan, G. Guisbiers, S. Pereira, M. R. Correia, P. Masri, A. Bruyant, S. Volz, and P. Royer, J. Appl. Phys. **107**, 083503 (2010).
[38] C. Jacoboni and L. Reggiani, Rev. Mod. Phys. **55**, 645 (1983).
[39] T. T. Tsong, Surf. Sci. **85**, 1 (1979).
[40] L. Arnoldi, E. P. Silaeva, A. Gaillard, F. Vurpillot, I. Blum, L. Rigutti, B. Deconihout, and A. Vella, J. Appl. Phys. **115**, 203705 (2014).
[41] Ioffe Physico-technical Institute, Electronic archive, http://www.ioffe.ru/SVA/NSM/Semicond/Si/.
[42] J. M. Hinckley and J. Singh, J. Appl. Phys. **76**, 4192 (1994).
[43] J. J. Letcher, K. Kang, D. G. Cahill, and D. D. Dlott, Appl. Phys. Lett. **90**, 252104 (2007).
[44] D.-s. Kim and P. Y. Yu, Phys. Rev. Lett. **64**, 946 (1990).
[45] L. C. Wang and H. J. Kreuzer, Surf. Sci. **237**, 337 (1990).